GAMMA-RAY SPECTROMETRY OF LDEF SAMPLES AT SRL

N92-23299

Willard G. Winn
Westinghouse Savannah River Company
Savannah River Site
Aiken, SC 29808
Phone: 803/725-2057 Fax: 803/725-3272

SUMMARY

A total of 31 samples from LDEF, including materials of aluminum, vanadium, and steel trunnions were analyzed by ultra-low-level gamma spectrometry. The study quantified particle induced activations of ^{22}Na, ^{46}Sc, ^{51}Cr, ^{54}Mn, ^{56}Co, ^{57}Co, ^{58}Co, and ^{60}Co. The samples of trunnion sections exhibited increasing activity toward the outer end of the trunnion and decreasing activity toward its radial center. The trunnion sections did not include end pieces, which have been reported to collect noticeable ^{7}Be on their leading surfaces. No significant ^{7}Be was detected in the samples analyzed.

The Underground Counting Facility at Savannah River Laboratory (SRL) was used in this work. The facility is 50 ft underground, constructed with low-background shielding materials, and operated as a clean room. The most sensitive analyses were performed with a 90%-efficient HPGe gamma-ray detector, which is enclosed in a purged active/passive shield. Each sample was counted for one to six days in two orientations to yield more representative average activities for the sample. The non-standard geometries of the LDEF samples prompted the development of a novel calibration method, whereby the efficiency about the sample surfaces (measured with point sources) predicted the efficiency for the bulk sample.

INTRODUCTION

Prior to retrieval of LDEF in January 1990, NASA Marshall Space Center initiated a program for radiometric analysis of the LDEF samples.[1] Due to extensive experience in ultra-low-level counting of environmental samples at the SRL Underground Counting Facility, NASA selected it as one of the laboratories for LDEF analyses. SRL received its first LDEF samples on March 7, 1990, and a total of 68 gamma spectrometry analyses were conducted on 31 samples submitted during 1990-1991. Round robin gamma analyses of these or similar samples were conducted at PNL, LNL, LBL, LLL, ORNL, TVA, and at NASA facilities in Houston, Texas and Huntsville, Alabama.

This report emphasizes the measurements of the induced radioactivity in the LDEF samples submitted to SRL, whereby it identifies particle reactions for producing the observed radionuclides, and examines trends within the data. These results will be used to appraise and improve models for characterizing trapped particles and cosmic rays.[2-4] A special emphasis is also given to the development of efficiencies for these somewhat unorthodox samples.

SYMBOLS

Symbols and units are given below. Efficiencies are unitless.

r,z	Cylindrical coordinates of sample (cm, cm)
$\epsilon(r,z)$	Gamma detection efficiency at sample point r,z
$\epsilon(r)$	Gamma detection efficiency of sample annulus r
ϵ	Gamma detection efficiency of sample
g(r)	Efficiency coefficient equal to $\epsilon(r,0)$
A,B,p	Constant in $\epsilon(r)$ fit of Equation 5 (–, cm^{-p}, –)
μ	Linear gamma attenuation coefficient (cm^{-1})
f	Average path length correction factor for μ (–)
c	Effective gamma geometric attenuation coefficient (cm^{-1})
U	$c + \mu f$ or total attenuation coefficient (cm^{-1})
U(r)	U expressed as function of r (cm^{-1})

MEASUREMENTS

The SRL Underground Counting Facility[5] was used to conduct gamma spectrometry on the LDEF samples. This facility is 50 ft below ground, and constructed with low-background materials. The 4 in. walls of the counting chamber are constructed of pre-World War II steel. The chamber is shielded by four to 7 ft of specular hematite. The total overburden is equivalent to 104 ft of water shielding, which reduces the cosmic background by an order of magnitude. Airborne particles are removed by filtering, classifying the facility as a Class 10,000 clean room. The very stable spectrometry electronics uses an uninterruptable power supply to protect against data losses during extended counting times.

HPGe detectors with standard efficiencies of 20%, 25%, and 90% were used in this study. A low-level lead shield encloses each detector and its sample cavity, which is purged of radon with the nitrogen that evaporates from its LN_2 dewar. The 90% HPGe has an inner shield of cadmium and copper to reduce X-ray backgrounds induced in the shielding by gammas from the sample. Figure 1 gives a typical background spectrum for this detector. Near the end of the study, the detector background was further reduced with an active plastic scintillator shield, which detects cosmic background events in anti-coincidence with the gamma counting to veto this background. In the present study, which used 1- to 6-day counting intervals, detection limits[6] for a ^{60}Co point source atop these detectors ranged from 0.04 to 0.4 pCi.

A total of 31 LDEF samples were examined by HPGe gamma spectrometry. The samples were trunnion disks and rectangular slabs of steel, vanadium, and aluminum. The disks had a diameter of 3.25 in. and 0.4 to 0.9 in. thickness; the slabs had maximum dimensions of 2 by 2 in^2 area and 0.35 in. thickness. Some of the slab samples were from radial layers of the trunnion disks. Each sample was counted with one side facing the detector, and then recounted with its other side facing the detector, so that activity distributions within the sample could be detected and averaged.

Detector efficiency calibration for the above samples used a method of mapping the point source efficiency over the sample surfaces. Point sources of ^{54}Mn, ^{57}Co, ^{60}Co, ^{133}Ba, and ^{137}Cs were used. Such a non-destructive calibration technique was important in this work because NASA required the samples be returned intact for round robin analyses at other laboratories.

ANALYSES

General

The HPGe data were collected as 4000 channel gamma spectra, as illustrated in Figure 1. The GRABGAM code,[5] which was developed at SRL for low-level counting, analyzed the spectra. This code uses three peak-area trapping windows, the largest of which is very sensitive for picking out peaks with low counting statistics. The peaks are examined as integral probability functions $F(x)$ per channel x to provide better statistics than afforded by fitting the peaks to differential probabilities $f(x)dx$. Such enhanced statistics are useful in characterizing the centroids and widths of low-level peaks. Following the analysis any peak contributions from the background spectrum are subtracted. The HPGe efficiency analyses procedures are overviewed in Figure 2 where methods for the trunnion disks and slab samples are outlined. Cylindrical coordinates r and z, relative to the sample, are used in the development of the HPGe efficiencies.

Trunnion Disks

Figure 2 depicts the counting geometry for a trunnion disk giving the point source locations used for calibration. Counting the point source at each location yielded an efficiency $\epsilon(r,z)$. The efficiency ϵ of a disk of uniform activity is the average of $\epsilon(r,z)$ over the disk volume V,

$$\epsilon = \frac{\int_V \epsilon(r,z)\ 2\pi r dr dz}{\int_V 2\pi r dr dz} \tag{1}$$

The only measured $\epsilon(r,z)$ are the $\epsilon(r,h)$ and $\epsilon(r,o)$ on the top and bottom surfaces of the disk; thus, a model is needed to infer the $\epsilon(r,z)$ within the disk. The model assumed in the present work was

$$\epsilon(r,z) = g(r)\ e^{-U(r)z} \tag{2}$$

where the z-dependence is exponential and the r-dependence is dictated by functions $g(r)$ and $U(r)$. An exponential is supported experimentally,[7] and it is shown to model both geometry and material absorption dependencies of the efficiency.[8]

Substituting Equation 2 into Equation 1 yields a ratio of radial area integrals.

$$\epsilon = \frac{\int_A \epsilon(r)\, 2\pi r dr}{\int_A 2\pi r dr} \quad , \tag{3}$$

where $\epsilon(r)$, resulting from integrals over z, is given by

$$\epsilon(r) = \frac{g(r)e^{-U(r)z}\,|_o^h}{-U(r)\,z\,|_o^h} = \frac{\epsilon(r,h) - \epsilon(r,o)}{\ln[\epsilon(r,h)/\epsilon(r,o)]} \quad . \tag{4}$$

Note that $\epsilon(r)$ is an exponential average along z *within* the sample volume, but it depends only on values $\epsilon(r,h)$ and $\epsilon(r,o)$ measured on the surface *outside* the volume.

Individual $\epsilon(r)$ were determined using Equation 4 with experimental measurements, and these values were fitted to a function

$$\epsilon(r) = A - B\, r^p \quad , \tag{5}$$

where A, B, and p are positive constants, and p is approximately equal to 2. Integrating this $\epsilon(r)$ in Equation 3 yields

$$\epsilon = A - [2/(2+p)]\, B\, a^p \quad , \tag{6}$$

where $r = a$ is the radius of the trunnion disk. Values of ϵ were determined as a function of energy, using the different point source standards. The resulting ϵ have better than 5% accuracy,[8] and refer to calibrations with standards from the National Institute of Standards and Technology.[9] The method directly calibrated the 20% HPGe and 25% HPGe detectors, which in turn cross-calibrated the 90% HPGe.

Metal Slabs

The 90% HPGe detector was used to appraise the low activities of the metal slabs. Efficiencies for these rectangular slabs were determined using techniques similar to those for the trunnion disks. However, because the slabs were smaller in area and thickness, an effectively constant $U(r) = U$ was assumed, consistent with experimental results,[7] so that Equation 2 could be expressed with separable variables in r and z, yielding

$$\epsilon(r,z) = g(r)\, e^{-U(r)z} = \epsilon(r,o)\, e^{-Uz} \quad . \tag{7}$$

When inserted in Equation 1, this $\epsilon(r,z)$ yields

$$\epsilon = \frac{\int_A \epsilon(r,o)\, 2\pi r dr}{\int_A 2\pi r dr} \quad \frac{\int_o^h e^{-Uz}\, dz}{\int_o^h dz} = \langle \epsilon(r,o) \rangle_A \quad \frac{1-e^{-Uh}}{Uh} \qquad (8)$$

where the first term is the numerical integrated average over the rectangular bottom surface, and the second term is integrated average over z. The point source mappings on the detector surface are used to determine the first term. The second term requires a knowledge of U, which may be expressed as

$$U = c + \mu f \quad , \qquad (9)$$

where c models the geometry dependence, and μf models the material absorption.[8] Here, the material attenuation coefficient μ is increased by a factor of f to correct for the average attenuation path, which is somewhat greater than z. The entire energy-dependence of U is primarily contained in μ, as c and f are essentially geometric parameters. Experimental measurements with sources of ^{54}Mn, ^{57}Co, ^{60}Co, and ^{137}Cs yielded U as a function of μ, to allow interpolation for predicting U for the other radionuclides. The μ for the gamma energies of these radionuclides were obtained from tabulations.[10] The resulting U were then used in Equation 8 to yield the slab efficiency ϵ.

A correction to ϵ needed to be developed for the ^{22}Na that was produced in the aluminum slabs, as its detected 1274 keV gamma peak is depleted by summing with its 511 keV annihilation gammas. Experimental measurements and calculations deduced that the observed 1274 keV count rate should be multiplied by a summing correction of 1.41 for the 90% HPGe detector.[8]

RESULTS

Trunnion disk sample results are summarized in Table 1. Specific activities are given for ^{7}Be, ^{46}Sc, ^{51}Cr, ^{54}Mn, ^{56}Mn, ^{57}Co, ^{58}Co, and ^{60}Co, where ^{54}Mn is dominant and ^{7}Be is only marginally detected at best. Here the results from counting both sides of the disk have been averaged to yield the values presented. Figure 3a plots the disk results for ^{54}Mn and ^{57}Co as a function of axial position along the trunnion, showing that these activities decrease as the position nears the LDEF end of the trunnion from the space end. Both trunnions were from the earth end of LDEF, where the LH-trunnion faced west, and the RH-trunnion faced east.

Trunnion radial layer activities are given in Table 2. The only significant radionuclides detected in these relatively small samples were ^{54}Mn and ^{57}Co. The results are the average from counting both sides of the sample. Figure 3b plots the layer results, showing that the activities increase with increasing radial position of the trunnion. The data also suggest that the radial profiles on the space side of the trunnion differ from

those on the earth side. The axial position of this RH–trunnion piece is 18 cm from its space end.

Vanadium and aluminum sample activities are presented in Table 2. Only ^{46}Sc was detected in the vanadium and only ^{22}Na was detected in the aluminum. Again, the activities are the average from counting both sides. The vanadium samples were from extreme LDEF locations, as the DISCUSSION will describe. The aluminum samples were from the keel plate and the end support retainer plate.

DISCUSSION

The LDEF samples examined in the present work implied cosmic activations induced by protons and neutrons. The trunnions imply activations as $^{14}N(p,2\alpha)^{7}Be$; $^{46}Ti(n,p)^{46}Sc$; $^{54}Fe(n,\alpha)^{51}Cr$; $^{56}Fe(p,2pn)^{54}Mn$; $^{58}Ni(p,2pn)^{56}Co$; $^{58}Ni(p,2p)^{57}Co$; $^{58}Ni(n,p)^{58}Co$; and $^{59}Co(n,\gamma)^{60}Co$. Actually, little if any ^{7}Be was observed. Noticeable ^{7}Be had been reported on samples with leading surfaces that can collect particles in the LDEF path,[11] but none of the samples analyzed at SRL had such surfaces. The only respective activations in the vanadium and aluminum samples were $^{51}V(p,*)\ ^{46}Sc$ and $^{27}Al(p,*)^{22}Na$, where spallation (*) reactions occurred.

Trunnions

The activities of ^{54}Mn and ^{57}Co decrease for axial positions closer to the LDEF body. The activities also decrease for decreasing radial position. Both decreasing trends are consistent with increased cosmic ray shielding. In addition, the LH or west–facing trunnion was activated somewhat more than the RH or east–facing trunnion; this is a signature of the trapped proton anisotropy in the South Atlantic Anomaly region.[3] The results are further supported by independent measurements on trunnions,[7] which are consistent for predictions for trapped and galactic protons.[4]

The data of Figure 3 also provide a self–consistency test between the modeled gamma efficiencies for the layer and disk samples. For the RHG section, its two radial activity profiles (earth side and space side) for ^{54}Mn were combined to yield their average radial profile, which was integrated to yield an activity of 79.8 pCi/kg for the RHG disk. This is consistent with the RH–trunnion trend of Figure 3 as the adjacent RHF disk activity was 78.98 ± 1.34 pCi/kg. Although the ^{57}Co radial profile is consistent with that of the ^{54}Mn, the imprecise data allow rather different profiles as well. However, no reasonable ^{57}Co profile yielded an integrated activity that was consistent with the trunnion trend in Figure 3. Specifically, the reasonable ^{57}Co profiles predicted a range of 10.5 to 13.7 pCi/kg for the RHG disk[8] while the adjacent RHF disk activity was 7.00 ± 0.59 pCi/kg.

The above comparison neglects the impact of the radial activity profile on the detection efficiency of the disk. Addressing this profile $p(r)$, the corresponding efficiency ϵ_p is given as

$$\epsilon_p = \frac{\int_A p(r)\,\epsilon(r)\,2\pi r dr}{\int_A p(r)\,2\pi r dr} \quad . \tag{12}$$

The tabulated disk values should be corrected by a factor of ϵ/ϵ_p. Using the activity profile of the RHG layers and the $\epsilon(r)$ measured for the adjacent RHF disk, an $\epsilon/\epsilon_p = 1.022$ was calculated[8] for ^{54}Mn. Applying this correction to the ^{54}Mn of the RHF disk yields 80.73 ± 1.37 pCi/kg compared with the 79.8 pCi/kg determined from the layers of the adjacent RHG disk. A similar treatment using the same $p(r)$ with the ^{57}Co $\epsilon(r)$ also yields a small correction, but this does not resolve the difference between the ^{57}Co layer and disk results. Apparently, a different $p(r)$ applies for ^{57}Co. Using a $p(r) = kr^2$ profile, which corresponds to the lowest reasonable profile–based activity of 10.5 pCi/kg for RHG, the resulting $\epsilon/\epsilon_p = 1.269$ for RHF yields 8.88 ± 0.75 pCi/kg. This illustrates that the ^{57}Co layer and disk results may become more consistent depending on the detailed nature of $p(r)$.

The trunnion disk results of Table 1 are all based on the assumption of uniform sample activities. Because appropriate ϵ/ϵ_p corrections are not generally available for these samples, such corrections were not applied. At the same time, a single available example for correcting ^{54}Mn illustrated a small correction in this case implying that ^{54}Mn values in Table 1 are reasonably accurate. Values for other radioisotopes of Table 1 can also be considered accurate if their corresponding $p(r)$ is in reasonable agreement with that for ^{54}Mn. However, caution should be exercised here, as the ϵ/ϵ_p examination for ^{57}Co implied a quite different $p(r)$, suggesting that the ^{57}Co of Table 1 might need to be increased by a factor of 1.6 ± 0.3. Finally, these observations suggest scrutiny in comparing round robin results from the different participating laboratories, because the ϵ determined for the various detectors will need to be corrected by their *different* ϵ/ϵ_p before precise agreement can be expected. Unfortunately, current experimental data appears insufficient for determining these ϵ/ϵ_p ; however, model predictions based on particle fluxes may be possible.[3,4]

Vanadium

The ^{46}Sc activated in vanadium indicated some trends; however, the photographs suggest that some of the samples may have been shielded so that only signatures of these trends are evident. The corresponding data of Table 2 is discussed below for signatures of anisotropic radiation received by the space/earth ends and east/west sides of LDEF.

The ^{46}Sc density of two samples (I–H12–VA and I–H12–VB) on the space end of LDEF was about 30% larger than that of a single sample (G12–A2–FNV) on the earth end; however, the error for the comparison is also about 30%. Because the photographs

imply that the space end samples were probably more shielded, the observation implies that the radiation received from the space side is greater. This is consistent with the earth acting as a cosmic shield for irradiation aimed at the earth end of LDEF.

The ^{46}Sc density of a sample (I-F2-V) on the west side of LDEF is only about 5% larger than that of a sample (I-C9-V) on the east side, and the error for the comparison exceeds 5%. However, the photographs imply that the sample on the west side is more shielded suggesting that the radiation from the west is higher. This is a signature of the South Atlantic Anomaly.[4]

Aluminum

The ^{22}Na activated in aluminum supports the anisotropic trends more dramatically than the vanadium results. The evidence for east/west and space/earth anisotropies are discussed below in logical order of development.

Two aluminum samples of the keel plate are on opposite sides of the keel, and tend to be shielded from each other by the keel. Consequently, one sample (KP-3) received radiation preferentially from the west, and the other (KP-10) from the east.[8] The ^{22}Na density of the west side sample was 48 $\pm$ 6% higher than that of the east side sample showing an unmistakable signature for the east/west anisotropy.

The keel itself is midway between the space and earth ends, so that the aluminum samples (KP-3 and KP-10) of the keel plate are closer to the space end than are the two samples (ESR-1 and ESR-2) of the retainer ring on the earth end.[8] The ^{22}Na densities of the two samples from the retainer ring agree having a difference of 1.2 $\pm$ 4.2%, as these samples were both unshielded and exposed to the same radiation. Both keel plate samples were partly shielded so that a hypothetical unshielded sample at this location would have ^{22}Na density in excess of either of the measured samples, but not more than their sum. Thus, the ^{22}Na density of the hypothetical unshielded keel plate sample would be 23 to 105% larger than that of the retainer ring samples indicating strong evidence for the space/earth anisotropy.

ACKNOWLEDGEMENTS

C. D. Ouzts is thanked for counting the LDEF samples and assisting with the development of the detector efficiency calibrations. Initial confirmation measurements supporting the efficiency model were provided by D. J. Lindstrom, NASA Johnson Space Center, Houston, Texas. Guidance and partial funding for this project were provided through the efforts of G. J. Fishman and B. A. Harmon, NASA Marshall Space Center, Huntsville, Alabama. Also, information contained in this work was developed during the course of work under Contract No. DE-AC09-89SR18035 with the U.S. Department of Energy.

REFERENCES

1. G. J. Fishman, T. A. Parnell, and B. A. Harmon, "Long Duration Exposure Facility (LDEF) Induced Radioactivity Plan", NASA Marshall Space Center, Huntsville, AL, Astrophysics Division, Space Science Laboratory Report, Dec. 1989.

2. E. V. Benton and W. Heinrich, "Ionizing Radiation Exposure on LDEF", University of San Francisco, San Francisco, CA, USF-TR-77, Aug. 1990.

3. T. W. Armstrong and B. L. Colborn, "Scoping Estimates of the LDEF Satellite Induced Radioactivity", Science Applications International Corp., Prospect, TN, SAIC-90/1462, Sep. 1990.

4. T. W. Armstrong and B. L. Colborn, "Radiation Calculations and Comparisons with Data", First LDEF Post-Retrieval Symposium, Kissimmee, Florida (June 2-8, 1991), NASA CP-3134, 1992.

5. W. G. Winn, W. W. Bowman, and A. L. Boni, "Ultra-Clean Underground Counting Facility for Low-Level Environmental Samples", *The Science of the Total Environment* Vol. 69, February 1988, pp. 107-144.

6. W. G. Winn, "Ultrasensitive Examination of Environmental Samples by SRL Underground Counting Facility", *Trans. Am. Nuc. Soc.* Vol. 54, June 1987, pp. 34-35.

7. C. E. Moss and R. C. Reedy, "Measurements of Induced Radioactivity in Some LDEF Samples", First LDEF Post-Retrieval Symposium, Kissimmee, Florida (June 2-8, 1991), NASA CP-3134, 1992.

8. W. G. Winn, "Gamma-Ray Spectrometry of LDEF Samples", Westinghouse Savannah River Company, Aiken, SC, WSRC-RD-91-16, Aug. 1991.

9. W. G. Winn and R. A. Sigg, "Pre-Operational Radio-Environmental Studies of Plant Vogtle", Westinghouse Savannah River Company, Aiken, SC, WSRC-RD-89-161 May 1, 1989.

10. K. Debertin and R. G. Helmer, *Gamma and X-ray Spectrometry with Semiconductor Detectors*, North-Holland, Elsevier Science Publishing Co., New York, 1988.

11. G. J. Fishman, B. A. Harmon, et al, "Observation of ^{7}Be on the Surface of LDEF Spacecraft", Nature, Vol 439, Feb. 1991, pp. 678-680.

Table 1. Trunnion Disk Results

Decay Correction Date – January 20, 1990

Sample	Isotopic Activities in pCi/kg Sample							
	Be-7	Sc-46	Cr-51	Mn-54	Co-56	Co-57	Co-58	Co-60
LHB	–	4.31 ±.59	–	120.21 ±1.53	4.58 ±.75	15.17 ±.73	3.31 ±1.15	1.96 ±.18
LHE	–	4.57 ±.71	–	95.21 ±1.75	2.92 ±.77	9.60 ±.66	1.33 ±1.35	1.59 ±.30
LHF	–	3.37 ±.51	–	100.50 ±1.41	4.84 ±.75	10.47 ±.63	4.06 ±1.16	1.40 ±.19
LHP	0.95 ±3.29	3.53 ±.20	16.38 ±7.38	79.43 ±.68	2.65 ±.21	7.48 ±.28	4.90 ±.33	1.58 ±.11
LHR	–7.48 ±3.65	3.78 ±.21	34.35 ±8.43	76.71 ±.68	2.66 ±.23	7.23 ±.36	4.68 ±.35	1.52 ±.11
LHS	2.56 ±3.28	4.34 ±.19	23.14 ±8.15	75.25 ±.59	2.53 ±.20	6.22 ±.25	4.92 ±.30	1.55 ±.09
RHB	–	5.04 ±1.00	–	82.52 ±1.36	3.21 ±.79	7.34 ±.59	4.67 ±1.27	1.39 ±.25
RHE	–	1.96 ±.75	–	79.77 ±1.57	2.15 ±.95	6.63 ±.57	2.35 ±1.27	1.16 ±.22
RHF	–	2.99 ±.64	–	78.98 ±1.34	3.75 ±.89	7.00 ±.59	2.45 ±1.26	1.32 ±.20
RHP	5.36 ±3.53	3.46 ±.21	35.22 ±8.84	72.56 ±.66	2.67 ±.22	7.28 ±.30	4.39 ±.33	1.45 ±.11
RHR	8.75 ±3.07	3.48 ±.19	26.16 ±8.13	72.75 ±.60	2.41 ±.19	6.20 ±.24	4.29 ±.30	1.55 ±.09
RHS	2.67 ±3.74	3.94 ±.23	31.89 ±10.08	74.66 ±.71	2.73 ±.25	6.01 ±.32	4.32 ±.41	1.44 ±.12

All errors are 1-σ counting errors

Table 2. Metal Slab Sample Results

Decay Correction Date: January 20, 1990

Space Side Trunnion Layers			Earth Side Trunnion Layers		
RHG-SP-	pCi/kg		RHG-ER-	pCi/kg	
	Mn-54	Co-57		Mn-54	Co-57
2	95.10 ±3.44	19.57 ±3.17	2	98.46 ±3.60	17.50 ±2.51
3	83.24 ±2.77	14.78 ±1.88	3	93.62 ±2.04	15.02 ±1.69
4	77.62 ±2.25	11.98 ±1.72	4	87.82 ±2.36	17.48 ±2.22
5	70.89 ±1.44	12.18 ±1.27	5	80.00 ±1.47	10.92 ±1.19
6	70.26 ±1.63	12.74 ±1.43	6	76.64 ±1.63	12.07 ±1.22

Vanadium	
Sample	pCi/kg Sc-46
G12-A2-FNV	16.00 ±1.32
I-C9-V	20.24 ±1.51
I-F2-V	21.12 ±2.70
I-H12-VA	19.82 ±12.84
I-H12-VB	21.59 ±6.77

Aluminum	
Sample	pCi/kg Na-22
ESR-1	90.60 ±3.31
ESR-5	91.70 ±1.94
KP-3	111.47 ±1.95
KP-10	75.33 ±2.60

All errors are 1-σ counting errors

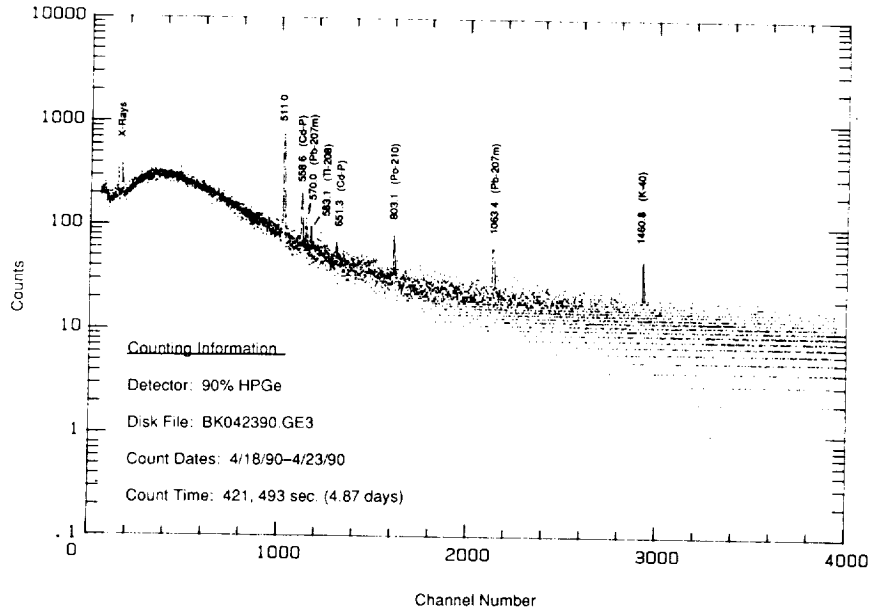

(a) Background

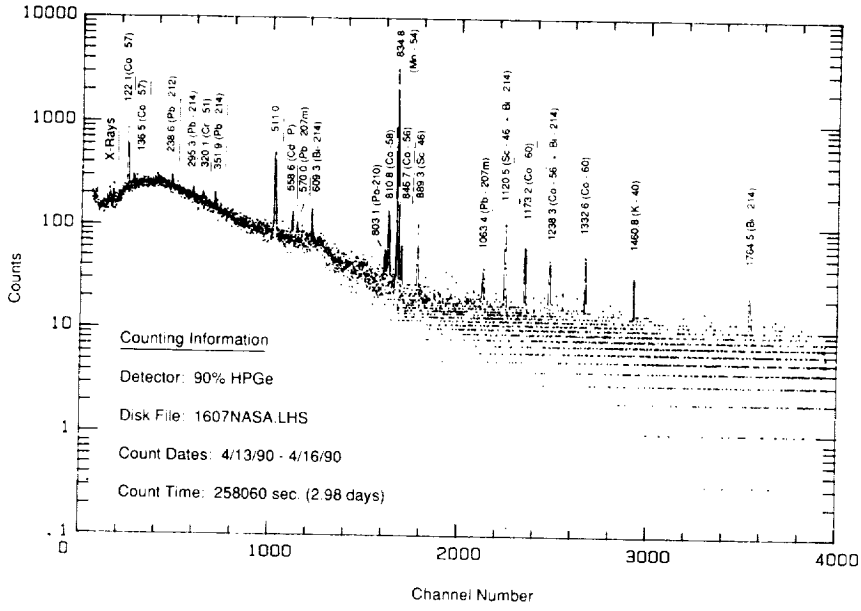

(b) Sample LHS

Figure 1. Typical Gamma-Ray Spectra

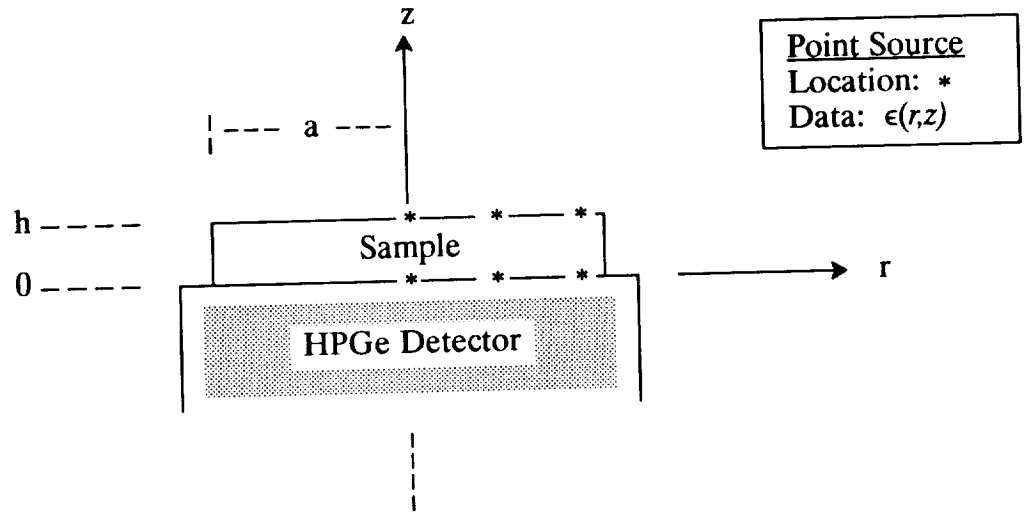

DISK ANALYSIS	SLAB ANALYSIS
(1) Exponential Average $\epsilon(r) = \frac{\epsilon(r,h) - \epsilon(r,0)}{\ln[\epsilon(r,h) / \epsilon(r,0)]}$	(1) Separable *r,z* Model $\epsilon(r,z) = \epsilon(r,0)\, e^{-Uz}$
(2) Radial Fitting $\epsilon(r) = A - Br^P$	(2) Sample Average $\epsilon(r,0)$ $<\epsilon(r,0)>_A$
(3) Sample Average $\epsilon = A - [2/(2+p)]Ba^P$	(3) Measure U/ Average e^{-Uz} $(1-e^{-Uh})/Uh$
	(4) Sample Average $\epsilon = <\epsilon(r,0)>_A (1-e^{-Uh})/Uh$

Figure 2. HPGe Efficiency Calibration

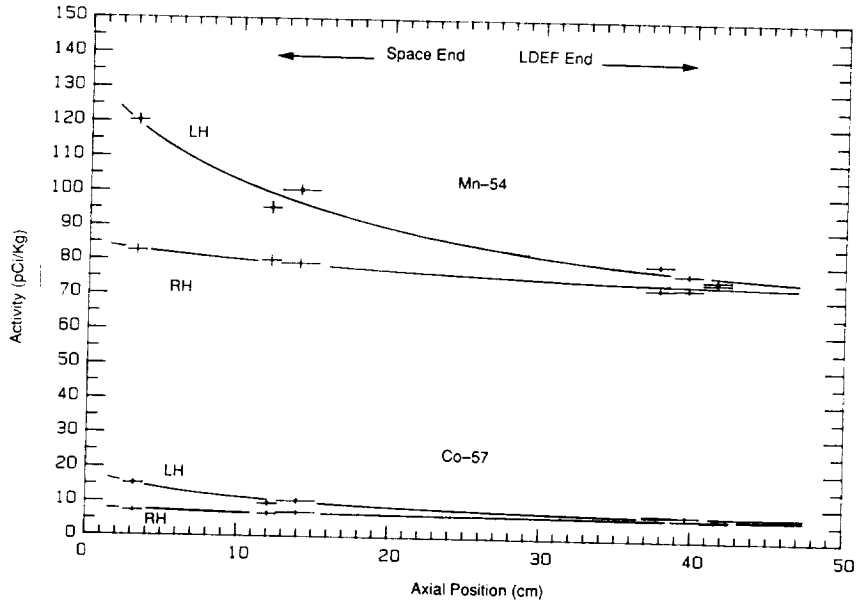

(a) LH and RH Samples B,E,F,P,R,S (plotted left-to-right)

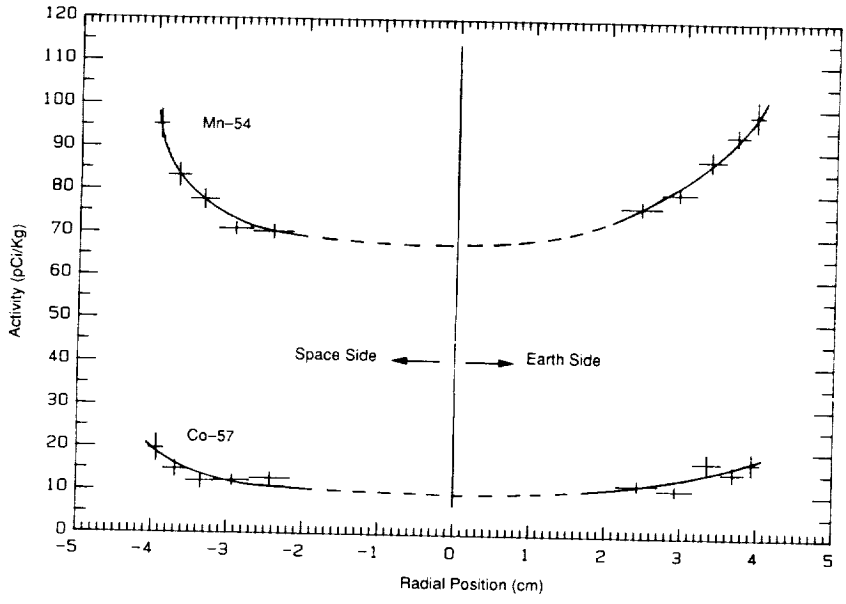

(b) RHG Samples

Figure 3. Results for Trunnion Samples